Journal of Thermal Analysis and Calorimetry
https://doi.org/10.1007/s10973-019-08996-x

# Evaluation of the thermal properties of $SrCO_3$-microencapsulated palmitic acid composites as thermal energy storage materials

**Ali Sobhani-Nasab[1,2] · Hossein Pourmohamadian[3] · Mehdi Rahimi-Nasrabadi[4,5] · Ghanbar Ali Sheikhzadeh[3] · Hassan Basirat Tabrizi[6]**

Received: 19 January 2019 / Accepted: 1 November 2019


## Abstract

A novel composite of $SrCO_3$-microencapsulated palmitic acid (PA) (PA@$SrCO_3$ microcapsules) was prepared an evaluated as a phase-change material through a self-assembly approach. Samples of the material were studied by Fourier transform infrared (FTIR) spectroscopy, X-ray diffractometery (XRD), scanning electron microscopy (SEM), and transmission electron microscopy (TEM) to determine the composition, crystalloid phase, microstructure, and morphology of the product. Also differential scanning calorimetry (DSC) and thermogravimetric analysis (TGA) were used to monitor the thermal behavior of the PA@$SrCO_3$ microcapsules. The data obtained through XRD and FTIR indicated the presence of characteristic peaks of PA and $SrCO_3$, which is only possible when the species do not chemically react with each other. SEM images indicated the PA@$SrCO_3$ microcapsules to be spheres with rough surfaces and average diameters of 1.5–2 μm. TEM images proved the samples as being composed of PA cores encapsulated in a $SrCO_3$ coating. The DSC results showed that the samples had phase-change behaviors, similar to those of pristine PA (melting point = 66.9 °C, latent melting heat = 48.8 J $g^{-1}$, freezing point = 55.7 °C, latent freezing heat = 43.2 J $g^{-1}$, at a microencapsulation ratio of 43.92%), and TGA results showed improvements in the thermal stability of PA@$SrCO_3$ microcapsules as opposed to PA, due to the presence of the $SrCO_3$ shell.

**Keywords** Microcapsule · Phase-change material · Palmitic acid · Thermal stability · Strontium (II) carbonate

## Introduction

The worldwide increase in energy consumption and the modern environmental problems pose a serious problem to energy supply industry. An approach to face such problems is using the unconventional and renewable energies and the development of efficient technologies and devices for different purposes including storage of energy, photocatalyst, supercapacitor, etc. [1–10].

PCMs are currently receiving considerable attention due to their applications in different fields areas like energy-saving materials for construction, storage and using of thermal solar energy, smart temperature-regulating fibers and textiles, cooling systems in electronic elements and instruments, wastewater treatment, low-temperature transportation units, solar plants, photovoltaic cells, and thermal management systems, etc. [11–13]. Based on their chemical natures, PCMs can are classified as organic, inorganic, or eutectics, and they can offer advantages or disadvantages in their thermal energy storage (TES) behaviors. In general, organic PCMs (OPCMs) are called TES systems, since they offer advantages including congruent melting/freezing profiles, low super-cooling, and vapor pressure changes at operating conditions, non-toxicity, and availability [14–16]. These PCMs are further classified into two main

✉ Mehdi Rahimi-Nasrabadi
rahimi@bmsu.ac.ir; rahiminasrabadi@gmail.com

1 Social Determinants of Health (SDH) Research Center, Kashan University of Medical Sciences, Kashan, Iran

2 Core Research Lab, Kashan University of Medical Sciences, Kashan, Iran

3 Mechanical Engineering Department, University of Kashan, Kashan, Iran

4 Chemical Injuries Research Center, Systems Biology and Poisonings Institute, Baqiyatallah University of Medical Sciences, Tehran, Iran

5 Faculty of Pharmacy, Baqiyatallah University of Medical Sciences, Tehran, Iran

6 Mechanical Engineering Department, Amirkabir University of Technology, Tehran, Iran

Published online: 14 November 2019

subclasses of paraffins and fatty acids. The latter show large latent heat capacities, excellent thermal conductivity, and small volume change through phase transition [17]. However, disadvantages like the small thermal conductivity, volume changes, leakage from capsules, low thermal response, flammability, and instability limit the possibility of directly using organic PCMs in heat storage applications. To overcome such shortcomings, the PCMs are packed in thin or shallow containers and/or clumping agents have been added to them [18, 19]. On the other hand, the process of microencapsulation which involves the physical or chemical trapping of 1–100 μm liquid or solid particles in a solid shell has been considered as a strategy for overcoming these defects. Microencapsulated structures, in which organic PCMs are enclosed in an inert material, can maintain a macroscopic solid form even under conditions in which the PCM core is molten [20–22]. This process further enhances the ease of handling organic PCMs and further the resulting microcapsules have large specific surface areas for more effective heat transfer [23].

A great deal of investigation has been performed on the preparation and properties of organic PCMs microencapsulated in different polymeric shells and examples of the conventional polymers used in the encapsulation process are poly(styrene-co-ethylacrylate) [19], polymethylmethacrylate [24], high-density polyethylene [25], polyurea [26], and melamine formaldehyde resin [27]. The polymeric shells might, however, cause environmental and/or health problems due to releasing toxic vapors, which poses serious limitations for using them in construction, medical, or food TES applications [20, 28]. Further, the thermal properties of the polymeric microcapsules like their flammability, low thermal and/or mechanical stability, or poor thermal conductivity can limit their application in different applications [20, 29].

Due to the disadvantages of polymeric shells, and given the advantages offered by inorganic materials in terms of non-flammability, thermal conductivity, mechanical, thermal, and chemical stabilities has attracted much attention to the area of microencapsulating OPCMs with inorganic or inorganic/organic hybrid shells [30, 31].

Studies have proven inorganic materials like $SiO_2$ [17], $Fe_3O_4/SiO_2$ [32], magnesium [33–35], and $TiO_2$ [36] to be proper encapsulating materials for OPCMs, and the resulting microcapsules have been reported to reveal good phase-change thermal behaviors, which have been attributed to the enhanced thermal conductivity. The structures also offer improved thermal stability, longer lives, and better sealing and anti-permeability properties, due to their presence of the rigid and compact shells [37]. In this regard, alkaline earth carbonates like $SrCO_3$ and $CaCO_3$ would be great candidates as inorganic shell due to their attractive properties especially their high thermal stability that lead to the increasing the durability and superior thermal conductivity. In this regard, there are some reports on using $CaCO_3$ as the shell material in constructing the PCMs, but to the best of our knowledge, there is no report on using $SrCO_3$ as inorganic shell [38–41].

Based on the above background, the present study was focused on preparing a $SrCO_3$-microencapsulated palmitic acid (PA) (PA@$SrCO_3$) through a self-assembly approach and evaluating the composition, crystalloid phase, and surface morphology of the product using FTIR, XRD, and SEM. Further, the thermophysical properties and thermal stability of the product were monitored through DSC and TGA.

## Experimental

### Materials

Palmitic acid (PA), TWEEN 80, Span 80 (served as the surfactants), petroleum ether $Sr(NO_3)_2$, and $K_2CO_3$ were supplied by Merck Co. and used as received.

### Preparation of samples

The typical method used for preparing the PA@$SrCO_3$ included adding 13.29 g of $Sr(NO_3)_2$ and 75 mL of deionized water to a beaker. In parallel, 10 g of PA, 0.65 g of TWEEN 80, and 0.35 g of Span 80 were mixed in 80 mL of DI water in a three-necked flask (250 mL). This mixture was stirred for a quarter at 80 °C, before the $Sr(NO_3)_2$ solution was gradually added to it in a drop-wise manner. The mixture was kept under stirring at 80 °C for 3 h. As a result, a stable oil/water emulsion was formed to which a solution of 9.7 g $K_2CO_3$ in 100 mL of DI water was added in a drop-wise manner in 60 min while being vigorously mixed at 1000 rpm. The resulting product, i.e., PA@$SrCO_3$, was eventually separated by centrifugation, washed with petroleum ether several times and then washed with deionized water. This white powder was next desiccated in a vacuum oven at 60 °C overnight. Three samples of the product were obtained at PA/$Sr(NO_3)_2$ mass ratios of 30/70, 40/60, and 50/50 by adjusting the stoichiometric ratios.

### Characterization of the samples

To acquire the XRD patterns a Philips X'pert MPD instrument with a CuKα radiation ($k = 0.15478$ nm) was used. The FTIR spectra were recorded in the range of 400–4000 $cm^{-1}$

on a PerkinElmer Spectrum 100 spectrophotometer, using KBr sheets. The field emission scanning electron microscopy studies on the samples were performed using a TESCAN MIRA3 microscope, and the TEM images were recorded on a Philips EM208S device.

To study the melting and freezing temperatures, as well as the latent heats of the different PA@$SrCO_3$ samples, DSC data were recorded on a S800 SPICO instrument under a constant stream of nitrogen, while heating or cooling 5 mg of the samples at 10 °C/min. 6 mg of the PA@$SrCO_3$ samples was used for the TGA analyses on a NETZSCH TG 209 F1 Iris thermal analyzer. The TGA analyses were performed in a nitrogen atmosphere at 20 °C/min starting from ambient temperature to 600 °C.

## Results and discussion

The PA@$SrCO_3$ samples were synthesized through the self-assembly method. Since PA is not water soluble, a stable PA/water emulsion was formed upon adding and dispersing PA, the surfactant containing water. In this suspension, the hydrophilic ends of the surfactants interact with the $H_2O$ molecules, while their hydrophobic segments of

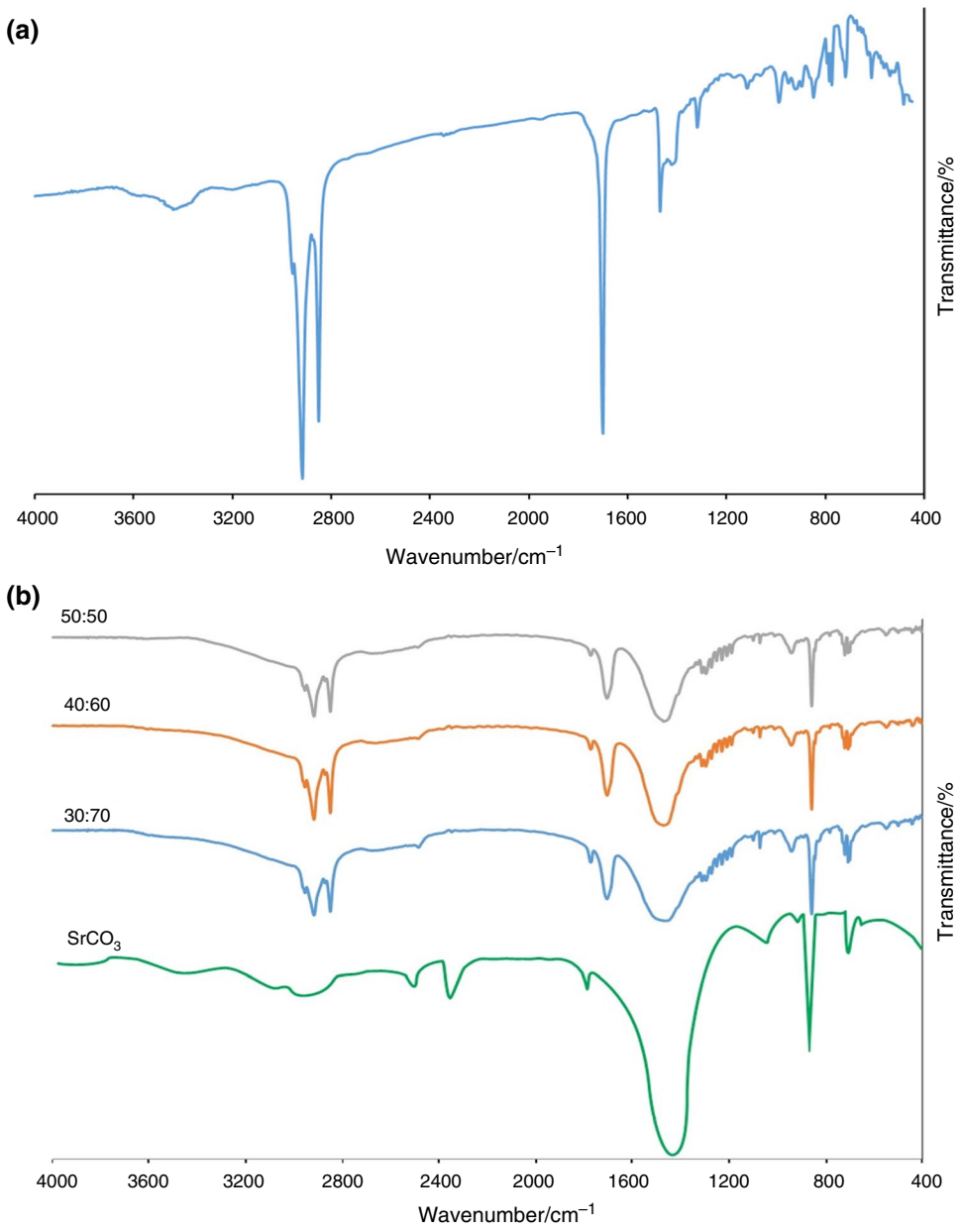


**Fig. 1** FTIR spectra of **a** pristine PA and **b** the microencapsulated PA synthesized with the PA/$Sr(NO_3)_2$ mass ratios of 50/50; 40/60, 30/70 and $SrCO_3$

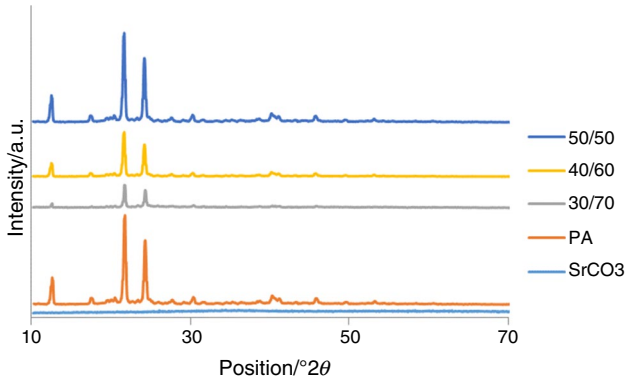


**Fig. 2** XRD patterns of (a) pristine PA and the microencapsulated PA synthesized with the PA/$Sr(NO_3)_2$ mass ratios of (b) 50/50, (c) 40/60, (d) 30/70, (e) $SrCO_3$

the molecules are oriented toward the droplets of PA, and as a result, a layer of the surfactants is formed around the PA droplets. Upon the drop-wise addition of the $Sr(NO_3)_2$ solution to the mixture, the metal cations can assemble on the surfactant layer, through interacting with the –OH groups present in the structure of the surfactant. Adding $K_2CO_3$ to this reaction mixture finally leads to the formation of the $SrCO_3$ shell.

FTIR studies were performed on the PA, $SrCO_3$, and PA@$SrCO_3$ samples, and the results are given in Fig. 1a–e. In the case of pristine PA (Fig. 1a), the bands at 2920 and 2855 $cm^{-1}$ correspond to the stretching vibrations of the $–CH_3$ and $–CH_2$ groups and that at around 1700 $cm^{-1}$ to the stretching of carbonyl (C=O) group. The band at 1320 $cm^{-1}$ can be attributed to the in-plane bending of the hydroxyl groups [42–44].

In the case of $SrCO_3$ (Fig. 1e), the absorptions at 836 and 560 $cm^{-1}$ are the result of the stretching vibrations of $CO_3^{2-}$ ions [45]. The signal at 1260–1670 $cm^{-1}$ corresponds to the C=O and the antisymmetric stretching of the C–O groups present in the $CO_3^{2-}$. The absorption band at 3200–3600 $cm^{-1}$ originates from the stretching and bending of the hydroxyl groups of the water molecules adsorbed on $SrCO_3$ [46]. For the PA@$SrCO_3$ samples (Fig. 1b–d), the bands typical to $SrCO_3$ and PA can be still observed at 1445 and 3400 $cm^{-1}$ and at 2920, 2855, and 1320 $cm^{-1}$, and no considerable new bands can be observed. The band corresponding to the stretching vibrations of C=O at 1471 $cm^{-1}$ is significantly decreased as compared to the FTIR spectrum of pristine PA (i.e., at 1700 $cm^{-1}$), which can be attributed to the strong interfacial interactions among the carboxyl group of the two components. This indicates the nature of the interactions among the two components (i.e., PA and $SrCO_3$) to be purely physical.

In general, making use of X-ray analysis is on the rise so that scholars can reach pure crystal structure of nanoparticles. [47–55]. In the case of pure PA, $SrCO_3$, and the different PA@$SrCO_3$ composites, the XRD patterns were obtained and are illustrated in Fig. 2a–e. Figure 2a contains five sharp peaks at $2\theta = 12.67°$, 21.83°, 24.32°, 30.37°, and 40.32°. These were, respectively, attributed to the diffractions of (110) and (200) crystal lanes of PA according to JCPDS No. 03 - 0250. Figure 2e, which was acquired for $SrCO_3$, contains a smooth peak at around 30–40, indicating the sample to be amorphous. As shown in Fig. 2b–d, the XRD patterns of the PA@$SrCO_3$ samples contain the characteristic peaks of PA and amorphous $SrCO_3$, only at lower intensities in comparison with those in Fig. 2c, d, further indicating the physical nature of the interactions among the ingredients [29].

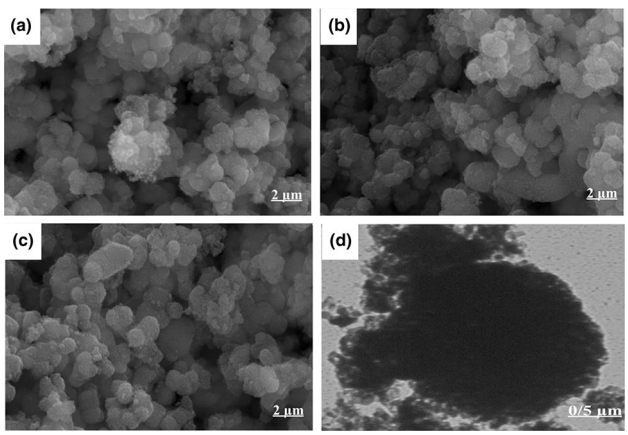


**Fig. 3** SEM micrographs of the microencapsulated PA synthesized with the PA/$Sr(NO_3)_2$ mass ratios of **a** 30/70, **b** 40/60, and **c** 50/50; **d** TEM micrograph of the microcapsules obtained at the PA/$Sr(NO_3)_2$ mass ratio of 50/50

The SEM and TEM images of the different composites are presented in Fig. 3, indicating all samples as being regular spheres with rough surfaces. The figures also indicate that some tiny particles were attached to the rough spheres. This can be due to the short induction period for strontium ions for assembly on the surface of the droplets, as a result of the inherently rapid precipitation of the salt. Figure 3d (TEM), to further demonstrate the product as being composed of PA cores and $SrCO_3$ shells, indicates the spheres as having diameters in the range of 1.0–1.5 µm. All of the observations supported the successful fabrication of the PA@$SrCO_3$ composite through the self-assembly method.

TGA is a powerful technique to determine the stability of inorganic and organic materials [49, 56]. TGA tests were performed to evaluate the thermal resistance and mass loss of PA, $SrCO_3$, and the PA@$SrCO_3$ (Fig. 4a–e).

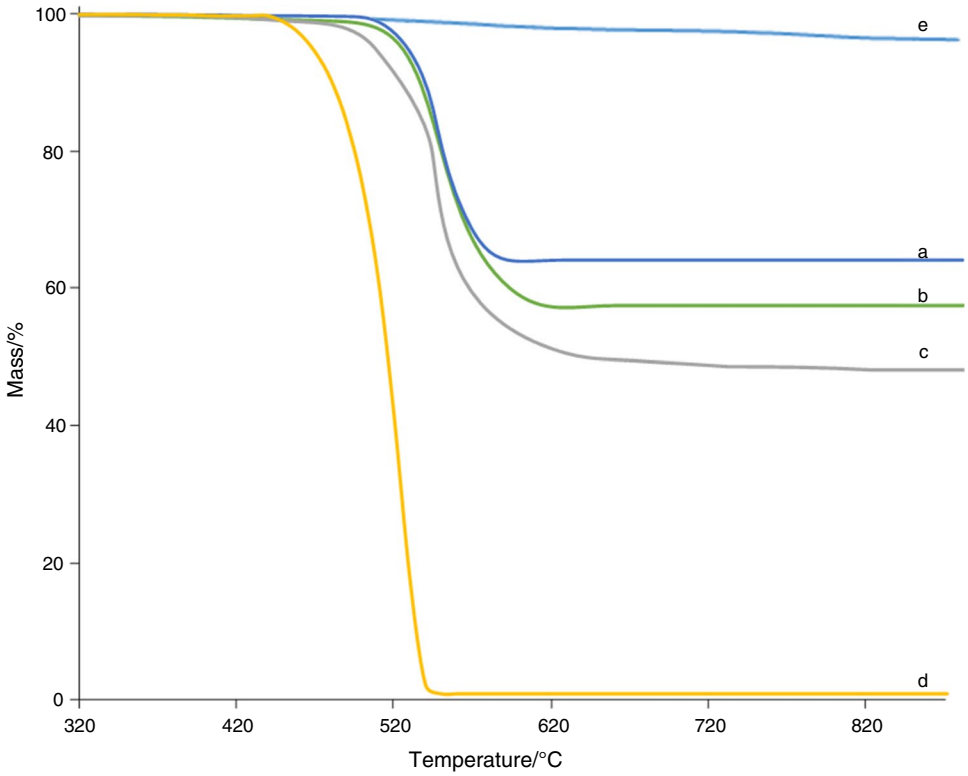


**Fig. 4** TGA curves of the microencapsulated PA synthesized with the PA/$Sr(NO_3)_2$ mass ratios of (a) 30/70, (b) 40/60, (c) 50/50 and (d) pristine PA and (e) $SrCO_3$

According to Fig. 4a, pristine PA undergoes a one-step mass loss process from 170 to 270 °C, and beyond this range, it does not lose any mass. As to PA@$SrCO_3$ microcapsules, the samples exhibited a two-step degradation behavior from 200 to 310 °C. This was attributed to the independent decomposition of the ingredients (i.e., PA and $SrCO_3$). Figure 4b–d clearly reveals that the PA in the PA@$SrCO_3$ samples has a lower maximum mass loss as opposed to pristine PA, as a result of the enhanced thermal stability through the $SrCO_3$-encapsulation. Figure 4e presents the TG analysis of $SrCO_3$. According to the result, the mass has not decreased, and therefore, $SrCO_3$ has great stability.

The phase-change profiles and latent heats of PA and the different PA@$SrCO_3$ samples were studied through DSC. Figure 5a, b illustrates the typical melting and freezing DSC curves, and evaluations on the thermal properties from the curves are given in Table 1. It is evident that pristine PA had single melting and freezing peaks at 67.2 °C and 56.5 °C, respectively. The behaviors of the different PA@$SrCO_3$ samples were rather similar to those of the pristine PA, supporting the physical nature of the interactions among the ingredients of the composites once more.

The 30:70 sample melted at 65.9 °C (latent heat = 36.4 J $g^{-1}$) and froze at 55.7 °C (latent heat = 24.4 J $g^{-1}$). In Table 1, it can be seen that the melting and freezing peak temperatures were lower those of pristine PA, for all composites. This could be due to higher specific surface areas of the microencapsulated composite in comparison with pristine PA. Also the microcapsules with a 50/50 core/shell mass ratio were found to have the highest melting and freezing latent heats among the three samples. The phase-change enthalpies of the composite samples were found to be directly proportional to the PA content of the samples.

Given the importance of the encapsulation ratio ($R$) and efficiency ($E$) in determining the thermal qualities of microcapsules, these values were calculated using the following equations and using the enthalpy determined through DSC [17], and the values are summarized in Table 1.

$$R = \frac{\Delta H_{\text{m, microcapsule}}}{\Delta H_{\text{m, PA}}} \times 100\% \quad (1)$$

$$\text{E} = \frac{\Delta H_{\text{m, microcapsule}} + \Delta H_{\text{f, microcapsule}}}{\Delta H_{\text{m, PA}} + \Delta H_{\text{f, PA}}} \times 100\% \quad (2)$$

$\Delta H_{\text{m,microcapsule}}$ and $\Delta H_{\text{f,microcapsule}}$ are the melting and freezing enthalpies of the product, and $\Delta H_{\text{m,PA}}$ and $\Delta H_{\text{f,PA}}$ are those of pristine PA, respectively.

The data in Table 1 show that the encapsulation ratio for the product with a 50/50 mass ratio was 39.44%, which is a bit lower than the loading content determined from the TGA results (46%). The encapsulation ratio

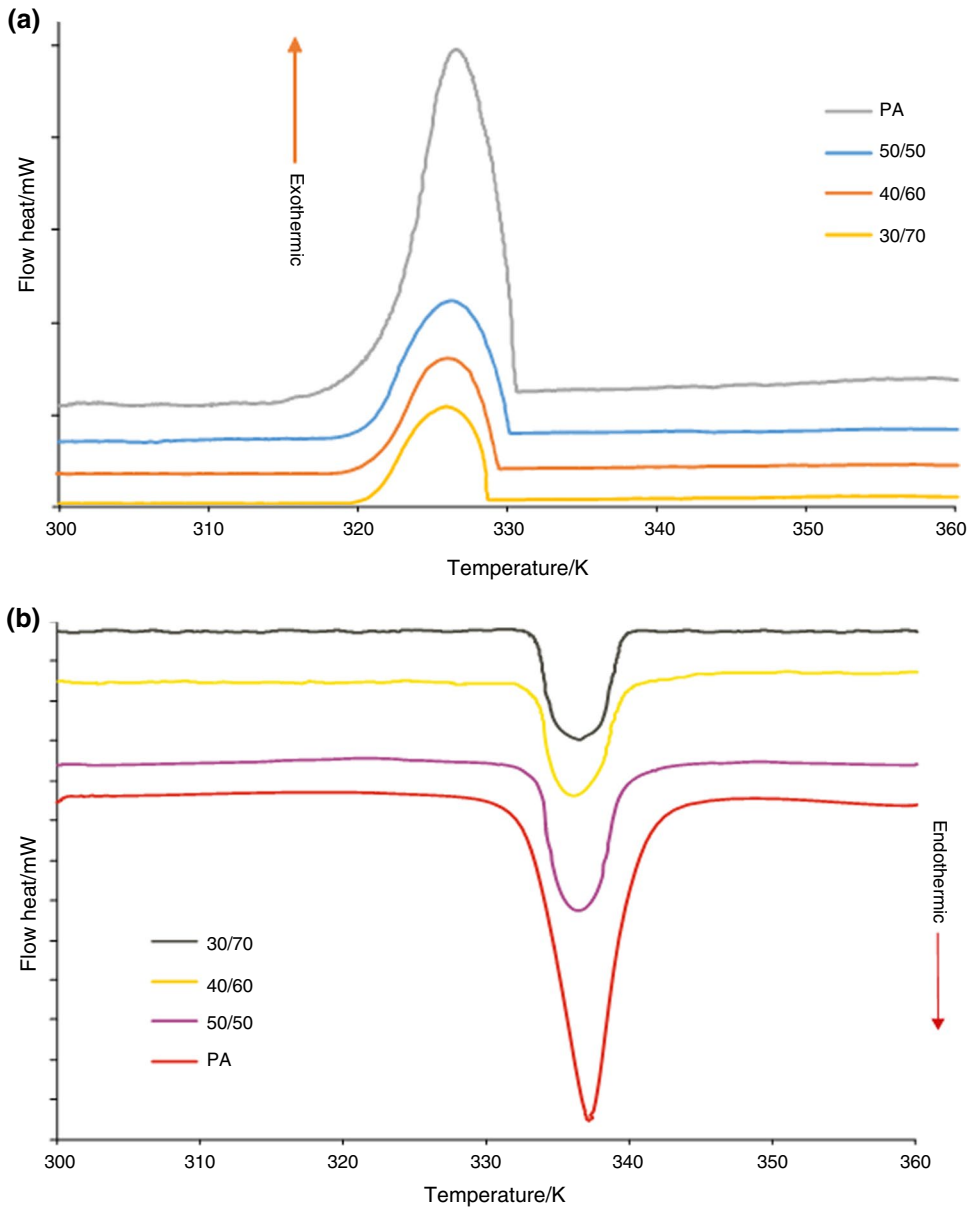


**Fig. 5** **a** DSC cooling curves and **b** DSC heating curves of pristine PA and the microencapsulated PA synthesized with different mass ratios of PA/$SrCO_3$

**Table 1** Phase-change behaviors of the microencapsulated PA synthesized with different mass ratios of PA/$Sr(NO_3)_2$

| Sample code | Mass ratio of PA/$Sr(NO_3)_2$ | Freezing process | | Melting process | | *R*/% | *E*/% |
|---|---|---|---|---|---|---|---|
| | | $T_f$/K | $\Delta H_f$/J $g^{-1}$ | $T_m$/K | $\Delta H_m$/J $g^{-1}$ | | |
| 1 | Pristine PA | 329.5 | 103.17 | 340.2 | 111.21 | – | – |
| 2 | 50/50 | 329.19 | 43.07 | 339.2 | 43.87 | 39.44 | 40.55 |
| 3 | 40/60 | 328.9 | 31.87 | 338.9 | 37.57 | 33.78 | 30.62 |
| 4 | 30/70 | 328.7 | 24.41 | 338.9 | 36.48 | 32.8 | 28.4 |

shows the effective encapsulation of the encapsulated PA for storing the latent heat. The loading content, on the other hand, indicates the total mass percent of PA in the microcapsules. So it can be concluded that not all of the microencapsulated PA are able to store the latent heat by phase change, and hence, the encapsulation ratio actually illustrates the effective performance of the microencapsulated PA.

## Conclusions

A microencapsulated PCM, based on PA core and $SrCO_3$ shell, was successfully prepared through a self-assembly approach. The product was studied using FTIR, XRD, SEM, TEM, TGA, and DSC. The FTIR and XRD result were indicative of physical interactions among the ingredients of the composite. The SEM and TEM images further revealed the microcapsule to be regular rough spheres of 1.0–1.5 µm in diameter. TGA studies revealed that the product undergoes a two-step degradation and that the presence of the organic shell improves the thermal stability of PA in the product. The DSC analyses proved the phase-change behavior of the composite to be very similar to that of the pristine PA, supporting the observations indicating the physical nature of the interaction among PA and $SrCO_3$ in PA@$SrCO_3$.

## References


1. Godarzi AA, Jalilian M, Samimi J, Jokar A, Vesaghi MA. Design of a PCM storage system for a solar absorption chiller based on exergoeconomic analysis and genetic algorithm. Int J Refrig. 2013;36(1):88–101.
2. Baniassadi A, Sajadi B, Amidpour M, Noori N. Economic optimization of PCM and insulation layer thickness in residential buildings. Sustain Energy Technol Assess. 2016;14:92–9.
3. Ahmadi F, Rahimi-Nasrabadi M, Behpour M. Synthesis $Nd_2TiO_5$ nanoparticles with different morphologies by novel approach and its photocatalyst application. J Mater Sci Mater Electron. 2017;28:1531–36.
4. Selvaraj V, Morri B, Nair LM, Krishnan H. Experimental investigation on the thermophysical properties of beryllium oxide-based nanofluid and nano-enhanced phase change material. J Therm Anal Calorim. 2019;137:1527–36.
5. Bhattad A, Sarkar J, Ghosh P. Hydrothermal performance of different alumina hybrid nanofluid types in plate heat exchanger. J Therm Anal Calorim. https://doi.org/10.1007/s10973-019-08682-y.
6. Peymani-Motlagh SM, Sobhani-Nasab A, Rostami M, Sobati H, Eghbali-Arani M, Fasihi-Ramandi M, Ganjali MR, Rahimi-Nasrabadi M. Assessing the magnetic, cytotoxic and photocatalytic influence of incorporating $Yb^{3+}$ or $Pr^{3+}$ ions in cobalt–nickel ferrite. J Mater Sci Mater Electron. 2019;30:6902–9.
7. Haibel E, Berendts S, Walter D. Thermogravimetric and X-ray diffraction investigation on carbonated lanthanum oxide and lanthanum hydroxide formed in humid CO2 atmosphere. J Therm Anal Calorim. 2018;134(1):261–7.
8. Rahimi-Nasrabadi M, Pourmohamadian V, Sadeghpour Karimi M, Naderi HR, Karimi MA, Didehban K, Ganjali MR. Assessment of supercapacitive performance of europium tungstate nanoparticles prepared via hydrothermal method. J Mater Sci Mater Electron. 2017;28:12391–8.
9. Sobhani-Nasab A, Behpour M, Rahimi-Nasrabadi M, Ahmadi F, Pourmasoud S. New method for synthesis of $BaFe_{12}O_{19}/Sm_2Ti_2O_7$ and $BaFe_{12}O_{19}/Sm_2Ti_2O_7$/Ag nano-hybrid and investigation of optical and photocatalytic properties. J Mater Sci Mater Electron. 2019;30(6):5854–65.
10. Sobhani-Nasab A, Rahimi-Nasrabadi M, Naderi HR, Pourmohamadian V, Ahmadi F, Ganjali MR, et al. Sonochemical synthesis of terbium tungstate for developing high power supercapacitors with enhanced energy densities. Ultrason Sonochem. 2018;45:189–96.
11. Babapoor A, Karimi G, Khorram M. Fabrication and characterization of nanofiber-nanoparticle-composites with phase change materials by electrospinning. Appl Therm Eng. 2016;99:1225–35.
12. Pomianowski M, Heiselberg P, Zhang Y. Review of thermal energy storage technologies based on PCM application in buildings. Energy Build. 2013;67:56–69.
13. Iten M, Liu S, Shukla A. A review on the air-PCM-TES application for free cooling and heating in the buildings. Renew Sustain Energy Rev. 2016;61:175–86.
14. Jiang B, Wang X, Wu D. Fabrication of microencapsulated phase change materials with TiO2/Fe3O4 hybrid shell as thermoregulatory enzyme carriers: a novel design of applied energy microsystem for bioapplications. Appl Energy. 2017;201:20–33.
15. Şahan N, Paksoy H. Determining influences of SiO2 encapsulation on thermal energy storage properties of different phase change materials. Sol Energy Mater Sol Cells. 2017;159:1–7.
16. Şahan N, Fois M, Paksoy H. The effects of various carbon derivative additives on the thermal properties of paraffin as a phase change material. Int J Energy Res. 2016;40(2):198–206.
17. Pourmohamadian H, Sheikhzadeh GA, Rahimi-Nasrabadi M, Tabrizi HB. Fabrication and characterization of microencapsulated PA with SiO2 shell through sol–gel synthesis via sodium silicate precursor. J Mater Sci Mater Electron. 2017;28(14):9990–7.
18. Pielichowska K, Pielichowski K. Phase change materials for thermal energy storage. Prog Mater Sci. 2014;65:67–123.
19. Alva G, Lin Y, Liu L, Fang G. Synthesis, characterization and applications of microencapsulated phase change materials in thermal energy storage: a review. Energy Build. 2017;144:276–94.
20. Song S, Dong L, Qu Z, Ren J, Xiong C. Microencapsulated capric–stearic acid with silica shell as a novel phase change material for thermal energy storage. Appl Therm Eng. 2014;70(1):546–51.
21. Fang G, Tang F, Cao L. Preparation, thermal properties and applications of shape-stabilized thermal energy storage materials. Renew Sustain Energy Rev. 2014;40:237–59.
22. Pourmortazavi SM, Babaee S, Ashtiani FS. Statistical optimization of microencapsulation process for coating of magnesium particles with Viton polymer. Appl Surf Sci. 2015;349:817–25.
23. Paulo F, Santos L. Design of experiments for microencapsulation applications: a review. Mater Sci Eng C. 2017;77:1327–40.
24. Huang J, Wang T, Zhu P, Xiao J. Preparation, characterization, and thermal properties of the microencapsulation of a hydrated salt as phase change energy storage materials. Thermochim Acta. 2013;557:1–6.
25. Guo X, Cao J, Peng Y, Liu R. Incorporation of microencapsulated dodecanol into wood flour/high-density polyethylene composite as a phase change material for thermal energy storage. Mater Des. 2016;89:1325–34.
26. Hirech K, Payan S, Carnelle G, Brujes L, Legrand J. Microencapsulation of an insecticide by interfacial polymerisation. Powder Technol. 2003;130(1–3):324–30.
27. Krupa I, Nógellová Z, Špitalský Z, Janigová I, Boh B, Sumiga B, et al. Phase change materials based on high-density polyethylene filled with microencapsulated paraffin wax. Energy Convers Manag. 2014;87:400–9.
28. Giro-Paloma J, Konuklu Y, Fernández A. Preparation and exhaustive characterization of paraffin or palmitic acid microcapsules as novel phase change material. Sol Energy. 2015;112:300–9.
29. Rahimi-Nasrabadi M, Ghaderi A, Banafshe HR, Eghbali-Arani M, Akbari M, Ahmadi F, et al. Preparation of $CO_2TiO_4/COTiO_3$/Polyaniline ternary nano-hybrids for enhanced destruction of

agriculture poison and organic dyes under visible-light irradiation. J Mater Sci Mater Electron. 2019;30(17):15854–68.
30. Li W, Zhang X-X, Wang X-C, Niu J-J. Preparation and characterization of microencapsulated phase change material with low remnant formaldehyde content. Mater Chem Phys. 2007;106(2–3):437–42.
31. Zhang X-x, Tao X-m, Yick K-l, Wang X-c. Structure and thermal stability of microencapsulated phase-change materials. Colloid Polym Sci. 2004;282(4):330–6.
32. Jiang F, Wang X, Wu D. Design and synthesis of magnetic microcapsules based on n-eicosane core and Fe3O4/SiO2 hybrid shell for dual-functional phase change materials. Appl Energy. 2014;134:456–68.
33. Pourmortazavi SM, Babaee S, Marashianpour Z, Kohsari I. Stabilizing of magnesium powder by microencapsulation with azidodeoxy cellulose nitrate. Prog Org Coat. 2015;81:107–15.
34. Mukhtar A, Nasir H, Rashid B, Waheed H. Development of zirconium and potassium perchlorate igniter for AP/HTPB composite propellant base bleed grain. J Therm Anal Calorim. https://doi.org/10.1007/s10973-019-08317-2.
35. Hu J, Wang C, Ren W, Zhang S, Liu F. Microstructure evolution and corrosion mechanism of dicalcium phosphate dihydrate coating on magnesium alloy in simulated body fluid. Mater Chem Phys. 2010;119(1–2):294–8.
36. Cao L, Tang F, Fang G. Preparation and characteristics of microencapsulated palmitic acid with TiO2 shell as shape-stabilized thermal energy storage materials. Sol Energy Mater Sol Cells. 2014;123:183–8.
37. Yu S, Wang X, Wu D. Microencapsulation of n-octadecane phase change material with calcium carbonate shell for enhancement of thermal conductivity and serving durability: synthesis, microstructure, and performance evaluation. Appl Energy. 2014;114:632–43.
38. Shi J, Wu X, Sun R, Ban B, Li J, Chen J. Synthesis and performance evaluation of paraffin microcapsules with calcium carbonate shell modulated by different anionic surfactants for thermal energy storage. Colloids Surf A. 2019;571:36–43.
39. Fakhrullin RF, Minullina RT. Hybrid cellular–inorganic core–shell microparticles: encapsulation of individual living cells in calcium carbonate microshells. Langmuir. 2009;25(12):6617–21.
40. Khosa AA, Zhao C. Heat storage and release performance analysis of CaCO3/CaO thermal energy storage system after doping nano silica. Sol Energy. 2019;188:619–30.
41. Bagherisereshki E, Tran J, Lei F, AuYeung N. Investigation into SrO/SrCO3 for high temperature thermochemical energy storage. Sol Energy. 2018;160:85–93.
42. Rahimi-Nasrabadi M, Behpour M, Sobhani-Nasab A, Jeddy MR. Nanocrystalline Ce-doped copper ferrite: synthesis, characterization, and its photocatalyst application. J Mater Sci Mater Electron. 2016;27(11):11691–7.
43. Asgarian SM, Pourmasoud S, Kargar Z, Sobhani-Nasab A, Eghbali-Arani M. Investigation of positron annihilation lifetime and magnetic properties of Co1–xCuxFe2O4 nanoparticles. Materials Research Express. 2018;6(1):015023.
44. Sobhani-Nasab A, Behvandi S, Karimi MA, Sohouli E, Karimi MS, Gholipour N et al. Synergetic effect of graphene oxide and C3N4 as co-catalyst for enhanced photocatalytic performance of dyes on Yb2 (MoO4) 3/YbMoO4 nanocomposite. In: Ceramics International; 2019.
45. Rahimi-Nasrabadi M, Pourmortazavi SM, Aghazadeh M, Ganjali MR, Sadeghpour Karimi M, Norouzi P. Fabrication, characterization and photochemical activity of ytterbium carbonate and ytterbium oxide nanoparticles. J Mater Sci Mater Electron. 2017;28:9478–88.
46. Rahimi-Nasrabadi M, Naderi HR, Karimi MS, Ahmadi F, Pourmortazavi SM. Cobalt carbonate and cobalt oxide nanoparticles synthesis, characterization and supercapacitive evaluation. J Mater Sci Mater Electron. 2017;28(2):1877–88.
47. Sobhani-Nasab A, Behvandi S, Karimi MA, Sohouli E, Sadeghpour Karimi M, Gholipour N, Ahmadi F, Rahimi-Nasrabadi M. Synergetic effect of graphene oxide and $C_3N_4$ as co-catalyst for enhanced photocatalytic performance of dyes on $Yb_2(MoO_4)_3$/$YbMoO_4$ nanocomposite. Ceram Int. 2019;45:17847–58.
48. Rahimi-Nasrabadi M, Pourmortazavi SM, Ganjali MR, Norouzi P, Faridbod F, Karimi MS. Statistically optimized synthesis of dyspersium tungstate nanoparticles as photocatalyst. J Mater Sci Mater Electron. 2016;27(12):12860–8.
49. Eghbali-Arani M, Sobhani-Nasab A, Rahimi-Nasrabadi M, Pourmasoud S. Green synthesis and characterization of $SmVO_4$ nanoparticles in the presence of carbohydrates as capping agents with investigation of visible-light photocatalytic properties. J Electron Mater. 2018;47(7):3757–69.
50. Rahimi-Nasrabadi M, Ahmadi F, Eghbali-Arani M. Different morphologies fabrication of $NiAl_2O_4$ nanostructures with the aid of new template and its photocatalyst application. J Mater Sci Mater Electron. 2017;28(3):2415–20.
51. Sobhani-Nasab A, Pourmasoud S, Ahmadi F, Wysokowski M, Jesionowski T, Ehrlich H, et al. Synthesis and characterization of MnWO4/TmVO4 ternary nano-hybrids by an ultrasonic method for enhanced photocatalytic activity in the degradation of organic dyes. Mater Lett. 2019;238:159–62.
52. Sedighi F, Esmaeili-Zare M, Sobhani-Nasab A, Behpour M. Synthesis and characterization of CuWO 4 nanoparticle and CuWO 4/NiO nanocomposite using co-precipitation method; application in photodegradation of organic dye in water. J Mater Sci Mater Electron. 2018;29(16):13737–45.
53. Khoshroo A, Hosseinzadeh L, Sobhani-Nasab A, Rahimi-Nasrabadi M, Ehrlich H. Development of electrochemical sensor for sensitive determination of oxazepam based on silver-platinum core–shell nanoparticles supported on graphene. J Electroanal Chem. 2018;823:61–6.
54. Sobhani-Nasab A, Rangraz-Jeddy M, Avanes A, Salavati-Niasari M. Novel sol–gel method for synthesis of PbTiO 3 and its light harvesting applications. J Mater Sci Mater Electron. 2015;26(12):9552–60.
55. Sobhani-Nasab A, Behpour M. Synthesis and characterization of AgO nanostructures by precipitation method and its photocatalyst application. J Mater Sci Mater Electron. 2016;27(2):1191–6.
56. Hajimirsadeghi S, Teimouri M, Rahimi-Nasrabadi M, Dehghanpour S. Non-isothermal kinetic study of the thermal decomposition of N-{bis [benzyl (methyl) amino] phosphoryl}-2, 2-dichloroacetamide and N-{bis [dibenzylamino] phosphoryl}-2, 2-dichloroacetamide. J Therm Anal Calorim. 2009;98(2):463–8.